2018 IEEE International Conference on Soft Robotics (RoboSoft)
Livorno, Italy, April 24-28, 2018

# State and Stiffness Estimation using Robotic Fabrics

Jennifer C. Case[1,2], Joran Booth[2], Dylan S. Shah[2], Michelle C. Yuen[1,2], and Rebecca Kramer-Bottiglio[2]

***Abstract*— Robotic fabrics are planar, fabric-based systems with embedded sensing and actuation functionalities. They are a useful, reconfigurable tool which can turn passive structures into active robots through surface-induced deformations. However, because of this flexibility, it is difficult to create empirical models for all possible configurations and host body materials that may be used with robotic fabrics. In this paper, we focus on the widely-applicable case of a continuum joint formed by wrapping a robotic fabric around a soft cylinder, and propose a model that is compatible with a variety of host body materials. The model is able take sensor data from the robotic fabric and then estimate both state and stiffness of the underlying structural material. We show the functionality of our model on three different materials: polyethelene foam, Dragonskin 10 Slow elastomer, and Smooth-Sil 935 elastomer. Simplified models that are able to provide both state and stiffness estimations are an important tool that can lead to advancements in control of soft robots.**

## I. INTRODUCTION

Soft robots have many applications, but are generally designed with a specific task in mind, such as locomotion [1]–[3], grasping [4]–[6], or manipulation [7], [8]. In order for soft robots to operate in unstructured environments, they will need to adapt to different environments, tasks, and interactions, and some examples of multifunctional [9]–[11] and reconfigurable [12], [13] soft robots have been shown. Here, we propose robotic fabrics. Robotic fabrics integrate both sensing and actuation elements with a fabric substrate, and can be wrapped around soft, passive bodies (*e.g.*, foams, elastomers, tensegrity structures, etc.) to impart motion onto those bodies. By reorienting a robotic fabric on the surface of a deformable body, or placing it on a different body with different properties and/or morphology, different motions and tasks may be achieved [14], [15].

Creating robots out of 2D fabrics has been previously demonstrated. Fabrics have been used to lighten a system while providing a yielding structure [16]. Our previous work includes demonstration of a fabric sensory sleeve that provides state estimation of an underlying 3D structure [17], as well as robotic fabrics that include variable stiffness actuating fibers [15] or integrated sensors and actuators [14]. In the latter work, the sensing elements in the robotic fabric were not sufficient to quantitatively estimate system state.

In this paper, we introduce a robotic fabric prototype containing conductive composite-based capacitive sensors and pneumatic McKibben actuators. We wrap this robotic fabric around passive cylindrical bodies to create active continuum joints (*i.e.*, actuators contract along the length of the cylinder). Further, we derive a corresponding analytical model that uses the sensors embedded within the fabric to estimate both state and stiffness of the underlying cylinder.

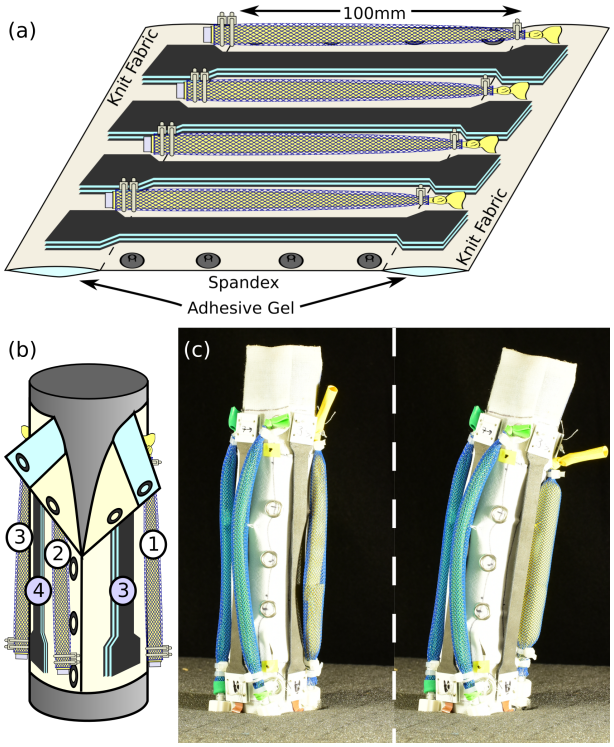


Fig. 1. (a) Sensors and actuators are placed on fabric in an alternating pattern to create a robotic fabric. Button snaps are placed on the sides and an adhesive gel is applied to the underside of the knit fabric. (b) The robotic fabric is wrapped around a passive body. The actuators are numbered in white while the sensors are numbered in color. (c) An example of a robotic fabric wrapped around and deforming a polyethene foam cylinder.

Robotic fabrics may be applied arbitrarily to passive host bodies, and the material properties of these bodies may not be known beforehand. Therefore, it is valuable to be able to retrieve that data from the robotic fabric itself. Here, our analytical model is applied to a relatively simple configuration to estimate the stiffness properties of the underlying host body by leveraging known actuator forces and system state. In the future, this work can be extended to more complex configurations and systems and could be used to generate system models that benefit feed-forward soft-bodied control approaches.

## II. MODEL

Our system consists of a robotic fabric with parallel actuators and sensors wrapped around a cylindrical deformable body (Fig. 1a-b). When an actuator contracts, it causes the

[1]School of Mechanical Engineering, Purdue University, West Lafayette, IN, USA
[2]School of Engineering & Applied Science, Yale University, New Haven, CT, USA

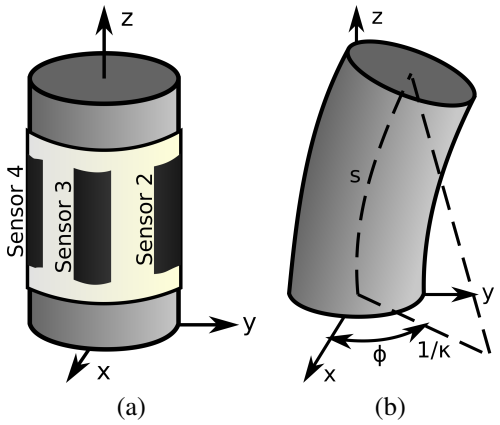


(a) (b)

Fig. 2. (a) Sensor placement. Sensors are placed at even intervals to align with the $x$- and $y$-axes. Sensor 1 is on the opposite side of sensor 3 behind the cylinder. (b) Schematic of a constant curvature beam.

cylinder to curve (Fig. 1c). To model this system, we first assume constant curvature, which allows us to adapt models developed for continuum robots [18], [19]. We further assume that no compression occurs along the central axis of the cylindrical body and that the system is not subject to external loads. Note that this model is dependent on sensor placement rather than type, and should therefore be extendable to other component choices regardless of the specific components implemented in this paper. Similarly, this model can be used for a variety of actuators as long as the exhibit contracting behavior required for the model.

### A. State Estimation

To estimate system state, we assume that the sensors in the robotic fabric follow the curvature of the bending cylinder (*i.e.*, perfect contact between the exterior fabric and internal body). Our robotic fabric prototype includes four evenly spaced sensors, which, when placed around the cylinder, can be used to define a coordinate frame such that the $x$- and $y$-axes align with the sensors (Fig. 2a). We define a segment with constant curvature in two ways: (1) using the length of the segment ($s$), curvature ($\kappa$), and angular offset of curvature ($\phi$); and (2) using the length of the segment ($s$), curvature along the $x$-axis ($\kappa_x$), and curvature along the $y$-axis ($\kappa_y$). We can convert between these two definitions using $\kappa = \sqrt{\kappa_x^2 + \kappa_y^2}$ and $\phi = \tan^{-1}(\kappa_y/\kappa_x)$. These variables are schematically shown in Fig. 2b.

With reliable data from all four sensors, we derive the system curvatures as:

$$\kappa_x = \frac{s_4 - s_2}{2sr_b}, \quad \kappa_y = \frac{s_1 - s_3}{2sr_b}, \tag{1}$$

where $s_i$ refers to the length of the $i$th sensor and $r_b$ is the radius of the cylindrical segment. Eqn. 1 assumes that all sensors are giving accurate information. However, unless the cylinder is being simultaneously strained and bent, it is likely that only two or three sensors are giving reliable data while the other sensors are buckled or slack. Using only two or three sensors, we we derive the system curvatures as:

$$\kappa_x = \frac{s_4 - s}{sr_b} = \frac{s - s_2}{sr_b}, \quad \kappa_y = \frac{s_1 - s}{sr_b} = \frac{s - s_3}{sr_b}, \tag{2}$$

where the appropriate equations are selected for determining $\kappa_x$ and $\kappa_y$, depending of the axis of curvature. Note that if there are three accurate sensors, a combination of equations can be selected from Eqns. 1 and 2 as needed.

### B. Stiffness Estimation

The state estimation model may be extended to also estimate the bending modulus or elastic modulus of the underlying material. Note that in order to estimate the stiffness, we must first estimate the state. For the stiffness estimation, we require at least one actuator that is placed parallel to the central axis of the body. Contracting this actuator will cause an equilibrium between the actuator force and the passive cylinder to be reached, which is dependent on the bending stiffness of the cylinder. We relate the bending stiffness ($K_b$) to the actuator force ($F$) as:

$$K_b = \frac{r_b F}{\kappa}. \tag{3}$$

Noting that $K_b = EI$, we can also determine the elastic modulus ($E$) of the material. We assume linear material properties, which has been previously validated using similar materials [20], and that the second moment of inertia ($I$) is known to calculate $E$ as:

$$E = \frac{r_b F}{I\kappa}. \tag{4}$$

## III. MATERIALS

The robotic fabric prototype implemented here employs a Spandex fabric substrate, capacitive sensors based on a conductive elastomer composite, and pneumatic McKibben actuators. Note that while we have miniaturized some pneumatic components [21], the purpose of this work is not to present an untethered system. Additionally, the model should be applicable to other types of actuation that operates on changes in length, such as cables and shape memory alloy coils, which may be easier to untether than pneumatics.

### A. Sensor Fabrication

The capacitive sensors were made from a conductive elastomer composite with expanded intercalated graphite (EIG), as described in [22]. Each sensor consisted of five alternating layers of conductive elastomer composite and inert elastomer, where the two outer layers of conductive elastomer composite were grounded to shield the sensor from environmental noise. The conductive elastomer composite was composed of Dragonskin 10 Slow (Smooth-On, Inc.) mixed with 10wt% EIG, and the inert elastomer was Dragonskin 10 Slow.

The sensors were fabricated via rod coating using a 1/2"-10 Acme threaded rod (97014A634, McMaster-Carr). First, a layer of conductive elastomer composite was coated onto a polyethylene terephthalate (PET) film (8567K12, McMaster-Carr) and cured. A subsequent layer of inert elastomer was coated on top, followed by another layer of conductive elastomer composite on just half the surface. A final inert layer was coated and allowed to partially cure until it was "tacky." The multilayer sheet was then folded over for tacky bonding, and a foam roller was used to remove air bubbles.

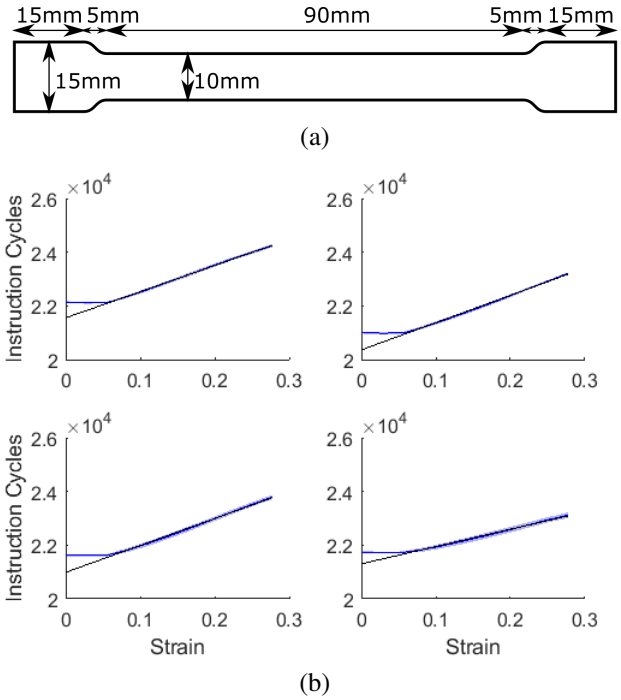


Fig. 3. (a) Sensor dimensions. (b) Instruction cycle-strain plots for the four sensors used on the robotic fabric. Each plot corresponds to one sensor. The average response is shown as a blue line. The colored clouds around the means represent the 95% confidence intervals for ten cycles. The black line represents a linear approximation of these data.

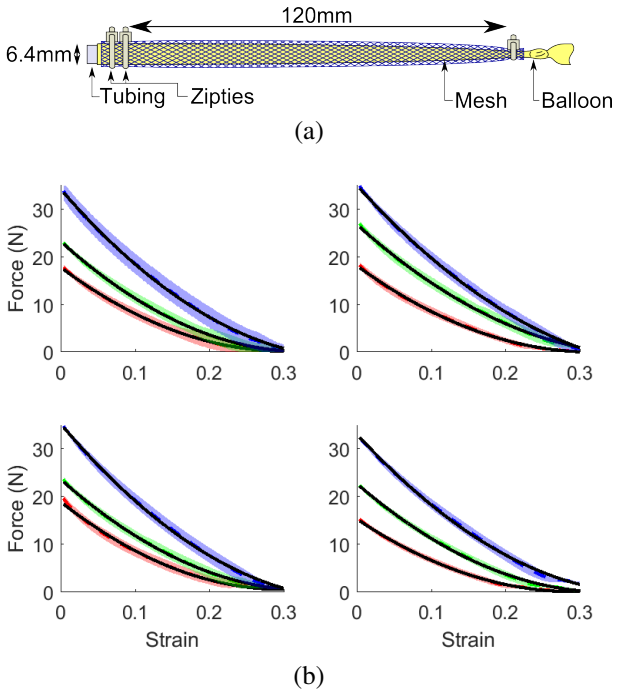


Fig. 4. (a) Schematic of actuator with dimensions given and parts labeled. Note the drawing is not to scale. (b) Force-strain plots for the four actuators used on the robotic fabric. Each plot corresponds to one actuator. The average response for the experimental data is shown as a dashed line of red for 69 kPa, green for 103 kPa, and blue for 138 kPa. The colored clouds around the means represent 95% confidence intervals for twelve cycles. The black lines represent a 2-degree polynomial fit of the average responses.

Once cured, the sensors were cut out using a 30 W $CO_2$ laser patterning system (VLS 2.30, Universal Laser Systems). The sensors were then removed from the PET film and cleaned of debris with soap and water. A staple was used to electrically connect the two grounded layers of the sensor. The sensors were connected to a signal conditioning board using strips of copper-coated Kapton (Pyralux, Adafruit). Dimensions of the sensors were chosen isolate the deformation to an active region that is 90 mm x 10 mm, as shown in Fig. 3a.

### *B. Actuator Fabrication*

To fabricate the McKibben actuators, a figure-8 knot was tied in one end of a latex balloon. The balloon was placed inside a 1/4" mesh (9284K2, McMaster-Carr) and a zip tie was placed just inside the knot to hold the mesh onto the balloon. Tygon tubing (6.4 mm outer diameter, 1.6 mm inner diameter) was inserted in the open end and two zip ties were applied to hold the mesh and balloon tight to the tubing. The McKibben actuators were controlled through a pressure regulator board. The resulting actuators are 120 mm in length fully stretched (Fig. 4a) and contract to approximately 85 mm when fully actuated.

### *C. System Integration*

The sensors and actuators were integrated with a fabric substrate. The fabric substrate consisted of a 100 mm x 120 mm spandex fabric section sewn to 20 mm x 120 mm knit fabric on either end. Spandex was chosen for the deformable section of fabric due to its high stretchability. Knit fabric was chosen for the ends because it stretches slightly in only one direction, which allows some uniaxial strain for wrapping around objects, but will not strain where the sensors and actuators are anchored.

The sensors and actuators were sewn in an alternating sensor-actuator pattern onto the knit part of the substrate such that they spanned the Spandex fabric. The sensors were pre-strained to 100 mm (from original length of 90 mm), while the actuators were pre-compressed to 100 mm (from original length 120 mm). This pre-compression was done to allow actuators to both stretch and compress while the system bends, since the model assumes both stretch and compression on the outer walls of the cylinder.

Button snaps were applied at the edges of the robotic fabric to allow attachment around a body. Finally, a coating of adhesive gel (Silbione RT gel 4717, Blue Star Silicones) was added to the knit fabric portions to help prevent slipping between the fabric and host body during actuation. The sensors and actuators were controlled with an Arduino Uno. The Arduino Uno acts as a slave for a Python script run on Lenovo Thinkpad laptop.

## IV. RESULTS & DISCUSSION

### *A. Sensor Characterization*

Sensors were characterized within the full robotic fabric system. The robotic fabric prototype was sewn to two brass rods on the top and bottom and loaded in a materials testing machine (3345, Instron). The robotic fabric was strain cycled 11 times starting at a length of 90 mm, which was the initial length of the sensors, and pulled to 120 mm, which was the limiting strain due to the actuators. The first strain cycle

TABLE I

PARAMETER VALUES FOR THE LINEAR FIT EQUATIONS THAT REPRESENT THE AVERAGE SENSOR RESPONSE. NOTE THAT SENSOR NUMBERING CORRESPONDS WITH FIG. 1B.

| | Sensor 1 | Sensor 2 | Sensor 3 | Sensor 4 |
|---|---|---|---|---|
| $a_0$ | 101 | 100 | 65 | 97 |
| $a_1$ | 20400 | 20900 | 21300 | 21600 |

was not included in the data analysis to remove the Mullin's effect [23]. The results from the ten sequent strain cycles were averaged together for each sensor and are shown in Fig. 3b. Note that the data from the sensors is reported here in instruction cycles, which is the number of instruction cycles the sensor's microprocessor goes through while the sensor charges and discharges (related to time to charge and discharge and, thus, the capacitance of the sensor). We implemented a linear fit ($IC = a_0\varepsilon + a_1$) for each sensor relating the sensor response to strain, where $IC$ represents instruction cycles from the sensor, $\varepsilon$ represents strain, and $a_i$ represent the parameters for the equation, which are given in Table I.

### B. Actuator Characterization

To measure the performance of the actuators, each one was placed in a materials testing machine (3345, Instron) and initially held at 120 mm for a given pressure. We sought to characterize true performance of the individual actuator, and not performance of the integrated robotic fabric, and therefore characterized the actuators before they were integrated into the robotic fabric. The actuators were strain cycled between 120 mm to 80 mm at 40 mm/min for 12 cycles. This test was repeated at different pressures: 69, 103, and 138 kPa. The first two cycles were discarded from the analysis since these involved breaking-in of the actuators. The results of this test can be seen in Fig. 4b. Although theory exists that describes the behavior of McKibben actuators, it does not account for friction or expansion of the balloon and differs from the actual performance significantly [24]. Therefore, we elected to use a 2-degree polynomial ($F = b_0\varepsilon^2 + b_1\varepsilon + b_2$) to represent the responses of our actuators, which matches the responses well. The parameters for this equation are given in Table II.

### C. State Estimation

In order to test the state estimation model, we wrapped the fabric around three different cylindrical body materials: polyethelene foam, Dragonskin 10 Slow elastomer ($E$ = 265 kPa), and Smooth-Sil 935 elastomer (Smooth On, Inc; $E$ = 536 kPa). Note that despite the fact that elastomers such as Dragonskin 10 Slow and Smooth-Sil 935 have a nonlinear stress-strain response, they have a linear response at low (<40%) strains [20]. The polyethelene foam was hollow with an outer diameter of 35.0 mm and an inner diameter of 18 mm. The two elastomers were solid with an outer diameter of 33.8 mm. The outer diameters correspond to $r_b$ in our model, while $s$ is 100 mm. The length of $s$ is determined by the "active" length of the fabric (*i.e.*, the 100 mm length of spandex).

TABLE II

PARAMETER VALUES FOR THE 2-DEGREE POLYNOMIAL EQUATIONS THAT REPRESENT THE AVERAGE ACTUATOR RESPONSE. NOTE THAT ACTUATOR NUMBERING CORRESPONDS WITH FIG. 1B.

| Actuator 1 | | | |
|---|---|---|---|
| kPa | $b_0$ | $b_1$ | $b_2$ |
| 69 | 192.6 | -116.5 | 17.9 |
| 103 | 214.8 | -141.1 | 23.3 |
| 138 | 229.3 | -180.3 | 34.3 |
| Actuator 2 | | | |
| kPa | $b_0$ | $b_1$ | $b_2$ |
| 69 | 179.5 | -114.2 | 18.2 |
| 103 | 181.2 | -140.4 | 26.9 |
| 138 | 193.8 | -171.9 | 35.1 |
| Actuator 3 | | | |
| kPa | $b_0$ | $b_1$ | $b_2$ |
| 69 | 207.0 | -123.5 | 19.0 |
| 103 | 206.5 | -138.8 | 23.7 |
| 138 | 232.9 | -185.1 | 35.4 |
| Actuator 4 | | | |
| kPa | $b_0$ | $b_1$ | $b_2$ |
| 69 | 179.4 | -104.7 | 15.4 |
| 103 | 200.1 | -135.1 | 22.8 |
| 138 | 216.1 | -170.1 | 33.2 |

The cylinder-robotic fabric system was placed vertically, as seen in Fig. 1, and two markers were placed along the central axis where the curvature occurred. Actuator 1, shown in Fig. 1b, was activated to a specific pressure after which a single sensor response was collected from all the sensors. Note that this data was collected with an Arduino Uno from each sensor's signal conditioning board. A photo was taken in each deformed configuration, which was used to generate truth state data. Deformation was repeated five times for a number of pressures (approximately 69, 103, 138, 172 kPa, or 10, 15, 20, 25 psi) for each cylinder, thus collecting five sensor responses and pictures at each position. The actual (truth) curvature of the system was determined from the photos using ImageJ, and the estimated curvature was calculated using the sensor data and our corresponding model. Specifically, we used data from sensors 1 and 4 to calculate the curvatures. Note that the sensor data was only used if it fell within the linear region of the sensor response (strain greater than 10%). Figure 5 shows the results of these tests.

Using the model to estimate state allows us to analyze a complex 3D deformation without the need for multiple sensor calibrations at various system positions. Rather, we can take advantage of pre-existing models and reform them around sensor data. However, as with any model, there are limitations, which can be seen in Fig. 5. The estimated curvature for the Dragonskin 10 Slow and Smooth-Sil 935 elastomer cylinders tracks fairly well, but there is a clear offset between the actual curvature and estimated curvature. In contrast, the estimated curvature for the foam cylinder gets decreasingly accurate with higher pressures, which is due to the material properties of the foam. While the sides of the elastomer cylinders are able to stretch and compress

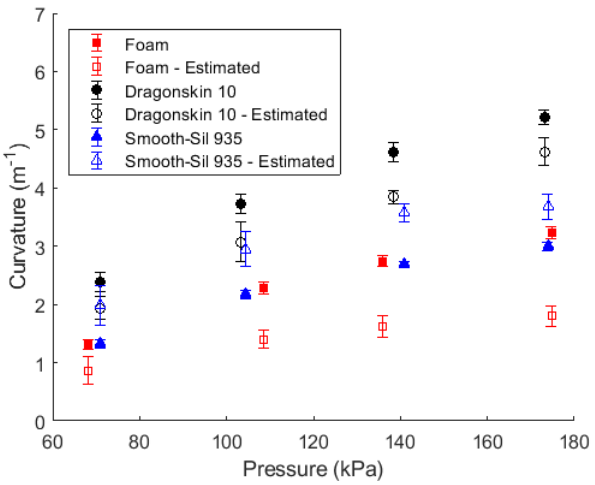


Fig. 5. Pressure-curvature data for the foam and elastomer cylinders. The curvature from the photos is shown as red filled squares, black filled circles, and blue filled triangles. The model estimation is shown as red hollow squares, black hollow circles, and blue hollow triangles. The error bars represent 95% confidence intervals.

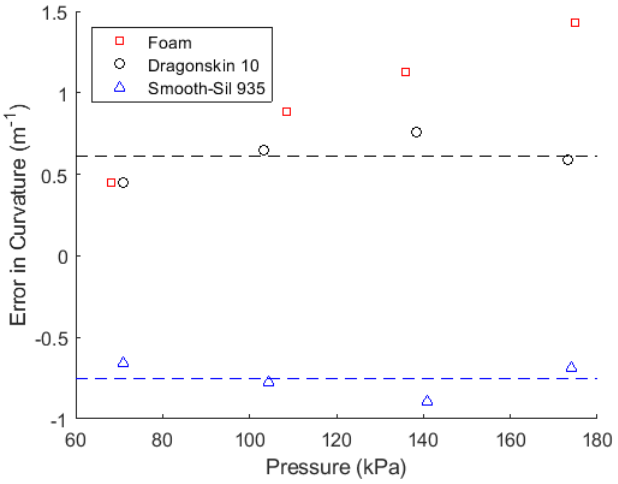


Fig. 6. Error in estimated and actual curvature. Fits for the data are shown as dashed lines.

as the cylinder bends, the foam cylinder can compress, but does not stretch as well as the elastomer. This means that the foam cylinder does not follow the assumptions of the model and, at most, the model is only useful at low pressures.

The errors between the mean estimated curvatures and mean actual curvatures can be seen in Fig. 6. Errors in the Dragonskin 10 Slow and Smooth-Sil 935 elastomer responses are nearly constant. Hence, we may add a final adjustment to our data to compensate for model error and improve the estimation by adding either our steady state error into model such that:

$$\kappa_{estimated} = \sqrt{\kappa_x^2 + \kappa_y^2} + e, \tag{5}$$

where $e$ is the constant error in the curvature for the elastomer cylinders. As an example, Fig. 7 shows the data adjusted for the observed error, which demonstrates that the model error can be corrected in practice to get more accurate

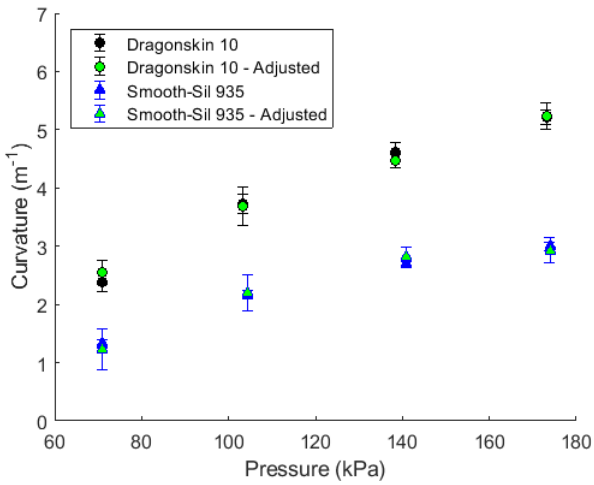


Fig. 7. Pressure-curvature data for the elastomer cylinders with the estimation data adjusted for the error. The adjusted model estimation is shown as black circles and blue triangles filled in with green for the foam and elastomer, respectively. The error bars represent 95% confidence intervals. This figure shows that in practice the error in the model can be compensated to get more accurate results.

TABLE III

ESTIMATED ELASTIC MODULUS AT VARIOUS PRESSURES. THE PERCENT ERROR IS DETERMINED FROM THE MEAN VALUE.

| | Dragonskin 10 Slow | | Smooth-Sil 935 | |
|---|---|---|---|---|
| Pressure (kPa) | $E_{est}$ (kPa) | % Error | $E_{est}$ (kPa) | % Error |
| 69 | $228 \pm 14$ | 14% | $655 \pm 240$ | 22% |
| 103 | $195 \pm 17$ | 26% | $459 \pm 91$ | 14% |
| 138 | $296 \pm 7$ | 12% | $640 \pm 51$ | 19% |
| **Avg** | **240±91** | **9%** | **585±242** | **9%** |

results.

### D. Stiffness Estimation

In order to estimate stiffness, we need to know the force from the actuator, which can be found using the force-strain equations from Table II. First, the length of the actuator ($s_{actuator}$) is found from our model as:

$$s_{actuator} = s(1 - \kappa r_b). \tag{6}$$

This length is then converted to strain and fed into the force-strain equation for Actuator 1 to get the approximate force.

With known forces, we used the adjusted curvature data from Fig. 7 along with Eqn. 4 to estimate the elastic modulus for both elastomers at pressures of 69, 103, and 138 kPa, and the results are shown in Table III. Notably, the estimated stiffness is most accurate (less than 10% error) when the results from all the tests are averaged together.

## V. CONCLUSION

In this paper, we have derived models to estimate the state and stiffness of a soft cylindrical body that is deformed from its surface by robotic fabric. The models leverage feedback from sensors embedded within the robotic fabric to estimate curvature state of the cylinder, and further use this state information alongside known actuator forces to

derive the elastic modulus of the cylinder material. We have evaluated the accuracy of the proposed models on representative cylinder body materials and found that the models are highly applicable across a range of curvatures for elastic materials, but only applicable at low curvatures for certain foam materials.

Simplified models that work with sensor data are necessary to track complex 3D movements of soft robotic systems. The state estimation model derived herein may be useful in the development of soft systems that utilize surface strains for information, such as sensory skins, robotic skins, and robotic fabrics. Integrated conformable systems that can manipulate arbitrary deformable bodies from their surface (*e.g.*, robotic fabrics) will further need to infer body material properties, such as stiffness, from the robotic fabric itself to inform system models and predict performance. In future work, we will expand our study to more materials and multiple samples of the same material to determine how robust the model is to changes, which will determine its usefulness in unstructured environments. Additionally, we can take advantage of a robotic fabric's ability to estimate the stiffness of its host body material within a feed-forward controller, which requires a known stiffness, alongside a sensory feedback controller, to help control the state of the system.

## ACKNOWLEDGMENT

This work was supported by the Air Force Office of Scientific Research under award number FA9550-16-1-0267. JCC and DSS are supported by NASA's Space Technology Research Fellowships (Grants NNX15AQ75H and 80NSSC17K0164, respectively). MCY is supported by a National Science Foundation Graduate Research Fellowship (Grant DGE-1333468).

## REFERENCES

[1] D. Drotman, S. Jadhav, M. Karimi, P. deZonia, and M. T. Tolley, "3d printed soft actuators for a legged robot capable of navigating unstructured terrain," in *2017 IEEE International Conference on Robotics and Automation (ICRA)*, pp. 5532–5538, May 2017.

[2] M. T. Tolley, R. F. Shepherd, M. Karpelson, N. W. Bartlett, K. C. Galloway, M. Wehner, R. Nunes, G. M. Whitesides, and R. J. Wood, "An untethered jumping soft robot," in *2014 IEEE/RSJ International Conference on Intelligent Robots and Systems*, pp. 561–566, Sept. 2014.

[3] M. Luo, Y. Pan, E. H. Skorina, W. Tao, F. Chen, S. Ozel, and C. D. Onal, "Slithering towards autonomy: a self-contained soft robotic snake platform with integrated curvature sensing," *Bioinspiration & Biomimetics*, vol. 10, no. 5, p. 055001, 2015.

[4] F. Ilievski, A. D. Mazzeo, R. F. Shepherd, X. Chen, and G. M. Whitesides, "Soft Robotics for Chemists," *Angewandte Chemie*, vol. 123, pp. 1930–1935, Feb. 2011.

[5] M. Manti, T. Hassan, G. Passetti, N. dElia, M. Cianchetti, and C. Laschi, "An Under-Actuated and Adaptable Soft Robotic Gripper," in *Biomimetic and Biohybrid Systems*, Lecture Notes in Computer Science, pp. 64–74, Springer, Cham, July 2015.

[6] K. C. Galloway, K. P. Becker, B. Phillips, J. Kirby, S. Licht, D. Tchernov, R. J. Wood, and D. F. Gruber, "Soft Robotic Grippers for Biological Sampling on Deep Reefs," *Soft Robotics*, vol. 3, pp. 23–33, Jan. 2016.

[7] A. D. Marchese, K. Komorowski, C. D. Onal, and D. Rus, "Design and control of a soft and continuously deformable 2d robotic manipulation system," in *2014 IEEE International Conference on Robotics and Automation (ICRA)*, pp. 2189–2196, May 2014.

[8] A. D. Marchese and D. Rus, "Design, kinematics, and control of a soft spatial fluidic elastomer manipulator," *The International Journal of Robotics Research*, p. 0278364915587925, Oct. 2015.

[9] A. A. Stokes, R. F. Shepherd, S. A. Morin, F. Ilievski, and G. M. Whitesides, "A Hybrid Combining Hard and Soft Robots," *Soft Robotics*, vol. 1, pp. 70–74, July 2013.

[10] M. Calisti, A. Arienti, F. Renda, G. Levy, B. Hochner, B. Mazzolai, P. Dario, and C. Laschi, "Design and development of a soft robot with crawling and grasping capabilities," in *2012 IEEE International Conference on Robotics and Automation*, pp. 4950–4955, May 2012.

[11] M. Calisti, M. Giorelli, G. Levy, B. Mazzolai, B. Hochner, C. Laschi, and P. Dario, "An octopus-bioinspired solution to movement and manipulation for soft robots," *Bioinspiration & Biomimetics*, vol. 6, p. 036002, Sept. 2011.

[12] S. W. Kwok, S. A. Morin, B. Mosadegh, J.-H. So, R. F. Shepherd, R. V. Martinez, B. Smith, F. C. Simeone, A. A. Stokes, and G. M. Whitesides, "Magnetic Assembly of Soft Robots with Hard Components," *Advanced Functional Materials*, vol. 24, pp. 2180–2187, Apr. 2014.

[13] S. A. Morin, Y. Shevchenko, J. Lessing, S. W. Kwok, R. F. Shepherd, A. A. Stokes, and G. M. Whitesides, "Using Click-e-Bricks to Make 3d Elastomeric Structures," *Advanced Materials*, vol. 26, pp. 5991–5999, Sept. 2014.

[14] M. Yuen, A. Cherian, J. Case, J. Seipel, and R. Kramer, "Conformable actuation and sensing with robotic fabric," in *2014 IEEE/RSJ International Conference on Intelligent Robots and Systems (IROS 2014)*, pp. 580–586, Sept. 2014.

[15] M. C. Yuen, R. A. Bilodeau, and R. K. Kramer, "Active Variable Stiffness Fibers for Multifunctional Robotic Fabrics," *IEEE Robotics and Automation Letters*, vol. 1, pp. 708–715, July 2016.

[16] A. Mehringer, A. Kandhari, H. Chiel, R. Quinn, and K. Daltorio, "An Integrated Compliant Fabric Skin Softens, Lightens, and Simplifies a Mesh Robot," in *Biomimetic and Biohybrid Systems*, Lecture Notes in Computer Science, pp. 315–327, Springer, Cham, July 2017.

[17] M. C. Yuen, H. Tonoyan, E. L. White, M. Telleria, and R. K. Kramer, "Fabric sensory sleeves for soft robot state estimation," in *2017 IEEE International Conference on Robotics and Automation (ICRA)*, pp. 5511–5518, May 2017.

[18] R. J. Webster and B. A. Jones, "Design and Kinematic Modeling of Constant Curvature Continuum Robots: A Review," *The International Journal of Robotics Research*, June 2010.

[19] M. W. Hannan and I. D. Walker, "Kinematics and the Implementation of an Elephant's Trunk Manipulator and Other Continuum Style Robots," *Journal of Robotic Systems*, vol. 20, pp. 45–63, Feb. 2003.

[20] J. C. Case, E. L. White, V. SunSpiral, and R. Kramer-Bottiglio, "Reducing Actuator Requirements in Continuum Robots Through Optimized Cable Routing," *Soft Robotics*, Oct. 2017.

[21] J. W. Booth, J. C. Case, E. L. White, D. S. Shah, and R. Kramer-Bottiglio, "An addressable pneumatic regulator for distributed control of soft robots," in *2018 IEEE International Conference on Soft Robotics (RoboSoft)*, 2018.

[22] E. L. White, M. C. Yuen, J. C. Case, and R. K. Kramer, "Low-Cost, Facile, and Scalable Manufacturing of Capacitive Sensors for Soft Systems," *Advanced Materials Technologies*, pp. n/a–n/a.

[23] L. Mullins, "Effect of stretching on the properties of rubber," *Rubber Chemistry and Technology*, vol. 21, no. 2, pp. 281–300, 1948.

[24] F. Daerden and D. Lefeber, "Pneumatic artificial muscles: actuators for robotics and automation," *European journal of mechanical and environmental engineering*, vol. 47, no. 1, pp. 11–21, 2002.